

Density Functional Theory for Hard Particles in N Dimensions

Stephan Korden

Institute of Technical Thermodynamics, RWTH Aachen University, Schinkelstraße 8, 52062 Aachen, Germany E-mail: stephan.korden@rwth-aachen.de

Version: March 11, 2014

Abstract: Recently it has been shown that the heuristic Rosenfeld functional derives from the virial expansion for particles which overlap in one center. Here, we generalize this approach to any number of intersections. Starting from the virial expansion in Ree-Hoover diagrams, it is shown in the first part that each intersection pattern defines exactly one infinite class of diagrams. Determining their automorphism groups, we sum over all its elements and derive a generic functional. The second part proves that this functional factorizes into a convolute of integral kernels for each intersection center. We derive this kernel for N dimensional particles in the N dimensional, flat Euclidean space. The third part focuses on three dimensions and determines the functionals for up to four intersection centers, comparing the leading order to Rosenfeld's result. We close by proving a generalized form of the Blaschke, Santalo, Chern equation of integral geometry.

Key words. integral geometry, Ree-Hoover diagram, Rosenfeld functional, fundamental measure theory

1. Introduction

Density functional theory (DFT) is a cornerstone of many-particle physics [5, 6]. But as of today, no systematic derivation for its functionals is known, neither in quantum nor in classical mechanics, turning its construction into a skill guided by symmetry considerations and perturbation theory. In the following, we will show that classical hard particles provide an exception to this rule.

Generally, a first approximation in the theory of inhomogeneous fluids is the splitting of the interaction potential into a soft contribution and an infinitely repulsive part, defining the particle's geometry and dominating the high density phase of soft matter [22]. Because of its singular potential, the hard-particle reference state cannot be treated perturbatively. Therefore, it was an important result, when Rosenfeld presented

a hard-sphere functional based on three observations: the decoupling of the Mayer function into a convolute of single-particle weight functions, the scaled-particle differential equation, and the overall scaling property of the free energy [30, 31, 32, 34].

Tarazona later showed the inconsistency of this first functional under restriction of the volume to layers, tubes, and single-particle caverns [44, 45]. But by adding further terms and two adjusted coefficients, the improved functional accurately described the phase diagram of mono-sized hard spheres. Following this strategy, more functionals have been proposed [38, 9, 41, 40] and successfully applied to several systems displaying nematic and crystalline phases [42, 1, 35, 36, 7, 8, 18, 21, 20]. Nevertheless, predictions of mixtures and systems of more complex geometries still remain limited to low densities.

Despite its success for spheres, the dependence of the fundamental measure theory (FMT) on the scaled particle equation, necessary for the non-perturbative map between low and high density, reduces the approach to a heuristic framework not extendable to higher order corrections. A first attempt to generalize the approach to further geometries than spheres has been taken by Wertheim, relating Rosenfeld's splitting of the Mayer function to the Gauss-Bonnet equation [47, 48, 49]. By calculating the third virial coefficient for ellipsoidal particles, he demonstrated the excellent agreement with numerical results, thus showing that the 'lost cases' of the Rosenfeld functional are a consequence of the single intersection center approximation [50].

Subsequently, the occurrence of the Gauss-Bonnet equation has been explained to be a consequence of the Blaschke, Santalo, Chern equation of integral geometry, whose generalization to arbitrary numbers of particles reproduces the weight densities entering in Rosenfeld's functional [17]. In combination with the virial expansion in Mayer diagrams, it also explained the polynomial structure of the functional and thus eliminated the dependence on the empirical scaled particle theory. It also showed that FMT actually defines an expansion of the exact functional in the number, or network, of intersection centers.

The current article completes this investigation. Starting with Sec. 2, it is shown that each intersecting network corresponds to a specific class of Ree-Hoover diagrams. Summing over all graphs of a class and determining their combinatorial prefactors, yields a generic functional, whose integrand factorizes into a convolute of integral kernels, one for each intersection center. The explicit form of this kernel is derived in Sec. 3, generalizing the Blaschke, Santalo, Chern equation in App. A. We close by presenting examples in Sec. 4.

2. The Virial Expansion

The decoupling of the Mayer function of hard particles into a convolute of 1-particle weight function dictates the further structure of the FMT functional which is independent of geometry and dimensions. This is discussed in Sec. 2.1 and motivates a change from particle to intersection coordinates. In Sec. 2.2 it is shown that this transformation requires a similar change of the virial expansion from Mayer to Ree-Hoover diagrams.

2.1. FMT as an expansion in intersection centers. Let us consider a set of $i = 1, \dots, N$ particles Σ_i imbedded into the finite subset V of the flat, Euclidean space $D_i : \Sigma_i \hookrightarrow V \subset \mathbb{R}^n$. In the thermodynamic limit $N, V \rightarrow \infty$, the particle density $\rho = N/V$ is kept constant, while the free energy $F(N, V, T)$ at temperature T becomes the function $F(\rho, T)$.

For more than one type of particle, the free energy generalizes correspondingly to $F(\{\rho_k\}, T)$ for a mixture of $k = 1, \dots, M$ compounds.

Following Hohenberg, Kohn, and Mermin, the thermodynamic equilibrium is defined as the minimum of the positive definite grand-canonical free energy $\Omega(\{\mu_k\}, T)$, a functional of the chemical potentials μ_k and the temperature T

$$\Omega(\{\mu_k\}, T) \geq \Omega(\{\mu_k^{(0)}\}, T) \geq 0, \quad (1)$$

where $\mu_k^{(0)}$ indicates the chemical potential at equilibrium state [22]. Taking into account possible external potentials $\phi_k(r)$ at $r \in \mathbb{R}^n$, the grand-canonical potential is related to the free-energy functional by the Legendre transformation in the local 1-particle densities $\rho_k(r)$:

$$\Omega(\{\rho_k\}, T) = F(\{\rho_k\}, T) + \sum_{k=1}^M \int \rho_k(r) (\phi_k(r) - \mu_k) d\gamma, \quad (2)$$

where we introduced the abbreviation

$$\begin{aligned} \Gamma(D) &:= \{\gamma = (r, \omega) \mid r \in D, \omega \in \text{SO}(n)\} \\ d\gamma_i &= d^n r_i d^{\frac{1}{2}n(n-1)} \omega_i \end{aligned} \quad (3)$$

for the differential volume element of the Euclidean group $\mathbb{E}^n = \mathbb{R}^n \ltimes \text{SO}(n)$.

However, the fundamental problem of the DFT approach is that, although the Hohenberg-Kohn theorem assures an almost unique relationship between interaction potential and free energy, it provides no hint for its derivation. It was therefore surprising, when the Rosenfeld functional could be derived from the virial expansion alone [17].

Substituting the Boltzmann function e_{ij} by Mayer's f-function $f_{ij} = e_{ij} - 1$ in the configuration integral and expanding the product in a series of cluster integrals, yields the virial representation of the free energy:

$$\begin{aligned} F = F_{\text{id}} + F_{\text{ex}} &= k_B T \sum_{k=1}^M \int \rho_k(r) (\ln(\rho_k(r) \Lambda_k^n) - 1) d\gamma \\ &+ k_B T V \sum_{n=2}^{\infty} \sum_{k_1, \dots, k_n=1}^M \int \frac{1}{n} B_n(\Gamma_n) \rho_{k_1}(r_1) \dots \rho_{k_n}(r_n) d\gamma_1 \dots d\gamma_n, \end{aligned} \quad (4)$$

with the “thermal wavelength” Λ_k of the kinetic part F_{id} . The excess energy F_{ex} is an infinite sum over virial integrals, depending on particle densities and sums over products of f-functions $B_n(\Gamma_n)$, with the Mayer clusters (also called diagram or graph) Γ_n representing an unordered sum over all labeled, 2-connected star-diagrams $\Gamma_{n,k}$ with $n \geq 2$ nodes and counting index k :

$$\Gamma_n = \sum_k \Gamma_{n,k}. \quad (5)$$

The number of graphs is a rapidly increasing function of n , whose asymptotic dependence for unlabeled diagrams has been estimated by Riddell and Uhlenbeck to be $2^{n(n-1)/2}/n!$ [46, 29]. This divergence of cluster integrals and the difficulties of their evaluation are the principal reasons why the virial approach is mostly limited to the gaseous state.

In order to go beyond the low-density limit, several alternative approaches have been developed. An early attempt has been taken by Reis, Frisch, and Lebowitz, resulting in the development of the scaled particle theory for hard spheres [28]. This approach is based on a heuristic but non-perturbative relation between the low- and high-density limit of the free energy and an analytic solution for the second virial integral [12, 15, 14]. Later on, this ansatz has been extended to convex particles based on results from Ishihara and Kihara, who derived B_2 in terms of Minkowski measures [23] and developed further by Rosenfeld into a local formulation in weight functions, suitable for density functionals [32]. However, the equivalence between the volume form of the Minkowski sum of domains and their respective intersection probability is strictly restricted to convex surfaces and limited to two particles. It, therefore, does not generalize to higher order virial clusters.

Starting from the f-function of hard particles, which is a negative step-function vanishing for non-intersecting domains D_i, D_j :

$$f_{ij} = \begin{cases} -1 & \text{if } D_i \cap D_j \neq \emptyset \\ 0 & \text{else} \end{cases} \quad (6)$$

Rosenfeld observed that its Fourier transformed integrand factorizes into 1-particle contributions. Transforming back, the Mayer function can be written as the sum over a convolute of distribution and tensor valued 1-particle weight functions:

$$f_{ij}(r_i - r_j) = - \int C^{A_i A_j} w_{A_i}^i(r_i - r_a) w_{A_j}^j(r_j - r_a) d\gamma_a, \quad (7)$$

with the constant and symmetric coefficient matrix $C^{A_i A_j}$ depending on the dimension of the imbedding space but otherwise independent of the particles' geometry. The transformation introduces the intersection coordinate $r_a \in D_i \cap D_j$ as a new variable relative to the particle positions and orientations $r_i \in D_i$. Here and in the following, we will omit the orientational dependence for the sake of clarity.

Rosenfeld's weight functions w_A^i are the local counterparts to the Minkowski measures of integral geometry [39, 43]. In 3 dimensions they depend on the normal vector \hat{n} , Gaussian curvature κ_G , mean curvature $\bar{\kappa}$, curvature difference Δ , surface σ , and the volume v :

$$\begin{aligned} w_G(r_i - r_a) &= \frac{1}{4\pi} \kappa_G \delta(\hat{n} r_a), & w_{\kappa L}(r_i - r_a) &= \frac{1}{4\pi} \bar{\kappa} \hat{n}^{\otimes L} \delta(\hat{n} r_a), \\ w_{\Delta L}(r_i - r_a) &= \frac{1}{4\pi} \Delta \hat{n}^{\otimes L} \delta(\hat{n} r_a), & w_{\sigma L}(r_i - r_a) &= \hat{n}^{\otimes L} \delta(\hat{n} r_a), \\ w_v(r_i - r_a) &= \Theta(\hat{n} r_a), \end{aligned} \quad (8)$$

where the L -fold tensor product of the normal vector $\hat{n}^{\otimes L}$ follows from a Taylor expansion of trigonometric functions, while the theta- and delta-functions restrict the integration to the volume, respective particle surface, as introduced in the appendix of [17].

Because the splitting (7) had originally been derived for spherical particles, its general dependence on Δ and the infinite set of tensor-valued weight functions had been obtained only later by Wertheim [47, 48, 49] and, independently by Mecke et al [7],

using the connection between (7) and the Gauss-Bonnet identity [33]. Wertheim also introduced the notion of n -point density functions [47,48]:

$$n_{A_1 \dots A_n}(r_{a_1}, \dots, r_{a_n}) = \sum_{i=1}^M \int w_{A_1}^i(r_i - r_{a_1}) \dots w_{A_n}^i(r_i - r_{a_n}) \rho_i(r_i) d\gamma_i \quad (9)$$

in which any Mayer integral can be rewritten. Given the example of the third virial integral

$$\begin{aligned} B_3 &= \frac{1}{6} \int f_{12} f_{23} f_{31} \rho_1 \rho_2 \rho_3 d\gamma_1 d\gamma_2 d\gamma_3 \\ &= -\frac{1}{6} C^{A_1 A_2} C^{B_2 B_3} C^{C_3 C_1} \int n_{A_1 C_1} n_{A_2 B_2} n_{B_3 C_3} d\gamma_a d\gamma_b d\gamma_c, \end{aligned} \quad (10)$$

Mayer clusters transform from a representation in particle positions and orientations to a corresponding representation in intersection coordinates $\gamma_i \rightarrow \gamma_a$.

Thus, instead of a virial expansion in increasing powers of 1-particle densities (4), the expansion in n -point densities suggests an ordering by their number of intersection centers [17]:

$$F_{\text{ex}} = k_B T V \sum_{n=1}^{\infty} \int \Phi_n(r_{a_1}, \dots, r_{a_n}) d\gamma_{a_1} \dots d\gamma_{a_n}, \quad (11)$$

whose leading order in 3 dimensions has the generic form:

$$\Phi_1(r_a) = -n_G \ln(1 - n_v) + C_{\alpha_1 \alpha_2} \frac{n_{\alpha_1} n_{\alpha_2}}{1 - n_v} + C_{\alpha_1 \alpha_2 \alpha_3} \frac{n_{\alpha_1} n_{\alpha_2} n_{\alpha_3}}{(1 - n_v)^2}, \quad (12)$$

where the volume dependence has been separated from the remaining densities $\alpha \in \{\kappa L, \Delta L, \sigma L\}$ and of which the Rosenfeld functional provides a first approximation [45]:

$$\begin{aligned} \Phi_1^{(R)}(r_a) &= -n_G \ln(1 - n_v) + \frac{n_{\kappa 0} n_{\sigma 0} - n_{\kappa 1} n_{\sigma 1}}{1 - n_v} \\ &\quad + \frac{1}{24\pi} \frac{n_{\sigma 0}^3 - 3n_{\sigma 0} n_{\sigma 1}^2 + \frac{9}{2}(n_{\sigma 1} n_{\sigma 2} n_{\sigma 1} - n_{\sigma 2}^3)}{(1 - n_v)^2}. \end{aligned} \quad (13)$$

The first two parts of this polynomial in the free-volume $1 - n_v$ is uniquely determined by the splitting of the second virial integral (7) and the scaled particle theory. The form of the third part, however, is only constrained by the scaling degree of the free-energy density. Several versions have therefore been proposed and tested, comparing its structure to analytical results and computer data [37]. Its exact form will be determined in Sec. 4.

2.2. Resummation of Ree-Hoover Diagrams. The expansion of the free-energy functional in intersection centers (11) is not well represented by Mayer diagrams. As can be seen from Fig. 1a), any intersection network of the ring diagram $\Gamma_{4,1}$ is also found in $\Gamma_{4,2}$ and $\Gamma_{4,3}$, thus contributing to Φ_1 , Φ_3 , and Φ_4 . This redundancy, which can be found for any diagram of identical number of nodes, explains an observation made by Ree and Hoover in their numerical investigations of Mayer integrals for spheres [24,26,25]. Ordering the n -particle virial integrals by their signs into positive and negative contributions $B_n = B_n^+ - B_n^-$, their individual parts are of comparable size $B_n^+ \simeq B_n^-$, but much

$$\begin{array}{lcl}
\Gamma_4 = +3 \begin{array}{c} \text{---} \square \text{---} \\ \text{---} \end{array} + 6 \begin{array}{c} \text{---} \square \text{---} \\ \text{---} \diagup \end{array} + 1 \begin{array}{c} \text{---} \square \text{---} \\ \text{---} \diagup \diagdown \end{array} & \tilde{\Gamma}_4 = +3 \begin{array}{c} \text{---} \square \text{---} \\ \text{---} \times \end{array} + 0 \begin{array}{c} \text{---} \square \text{---} \\ \text{---} \diagup \diagdown \end{array} - 2 \begin{array}{c} \text{---} \square \text{---} \\ \text{---} \diagup \diagdown \end{array} \\
\text{a) } = \Gamma_{4,1} + \Gamma_{4,2} + \Gamma_{4,3} & \text{b) } = \tilde{\Gamma}_{4,1} + \tilde{\Gamma}_{4,2} + \tilde{\Gamma}_{4,3}
\end{array}$$

Fig. 1. The fourth virial diagrams in Mayer Γ_4 and Ree-Hoover $\tilde{\Gamma}_4$ representation: a) The slow convergence of the virial expansion is partly explained by identical intersection patterns in Mayer diagrams of equal order. b) Ree-Hoover diagrams resolve this problem. With the additional Boltzmann functions, the allowed intersection of particles are constrained. Additionally, the symmetry factors of many diagrams vanish, thus reducing the overall number of integrals entering the virial expansion.

larger than B_n itself, often by two orders of magnitude [24]. Thus, in order to reduce the number of redundant intersection patterns, they inserted the identity $1 = e_{ij} - f_{ij}$ for any pair of nodes i, j not bonded by an f-function. The resulting Ree-Hoover (RH) diagrams are completely connected graphs of f- and e-bonds, as shown in Fig. 1b). The type of allowed intersections is therefore constrained and comes close to the graphical interpretation of FMT functionals as intersection networks. In the following, we will show that this representation not only significantly simplifies our previous derivation, but also allows the systematic generalization of the approximate free-energy functional to higher orders.

The previous analysis of the Rosenfeld functional started from the observation that its dependence on a single intersection center can only be related to diagrams which allow the particles to intersect in a common point. While this involves all Mayer clusters, it selects the subclass of RH-graphs without e-bonds. It therefore establishes a one-to-one relation between its elements of the virial series and the exclusively f-bonded RH-clusters, with their integration domains restricted to a single intersection center. This relation can now be used as a guideline for the construction of higher order functionals, summarized in four steps: 1. choose an intersection network and find the corresponding class of RH-diagrams, 2. determine their symmetry factors and 3. intersection probabilities, and 4. sum over all elements of the class. In the remaining part of the current section, we will focus on the first two subtopics, saving the last two items to Sec.3.

For the two classes of Mayer and RH-diagrams, we introduce the following conventions:

Definition 1 Let $\Gamma_{n,k}$ denote a labeled, 2-path connected Mayer diagram (star-graph) of n nodes and $|\Gamma_{n,k}|$ f-bonds. Two Mayer graphs are subgraphs $\Gamma_{n,k} \subseteq \Gamma_{n,k'}$ if they agree after removing a finite number of f-bonds from $\Gamma_{n,k'}$.

A node can be removed by deleting its vertex with all its bonds $\pi^{-1} : \Gamma_{n,k} \rightarrow \{\Gamma_{n-1,k'}, \Gamma_{n-1,t}^A\}$, resulting in a residual diagram which is either a new star-graph $\Gamma_{n-1,k'}$ or a linear chain with articulation points $\Gamma_{n-1,t}^A$.

Definition 2 Let $\tilde{\Gamma}_{n,k}$ be a RH-diagram with n nodes and $|\tilde{\Gamma}_{n,k}|$ f-bonds.

A node, which is only linked by f-bonds, can be removed from a diagram by deleting its vertex and all its bonds, leaving either a new or the trivial RH-graph $\pi^{-1} : \tilde{\Gamma}_{n,k} \rightarrow \{\tilde{\Gamma}_{n-1,k'}, 0\}$.

Two RH-graphs are subgraphs $\tilde{\Gamma}_{n-m,k'} \subseteq \tilde{\Gamma}_{n,k}$ if they are related by $\pi^{-m} = (\pi^{-1})^m$.

Definition 3 Mayer- and RH-graphs are subgraphs, $\Gamma_{n,k} \subseteq \tilde{\Gamma}_{n,k'}$, $\tilde{\Gamma}_{n,k} \subseteq \Gamma_{n,k'}$, if they agree after removing a finite number of f-bonds and deleting all e-bonds.

Because the application of π^{-1} on a RH-graph maps to exactly one element, its inverse operation $\pi : \tilde{\Gamma}_{n-1,k} \rightarrow \tilde{\Gamma}_{n,k'}$ can be defined for $\tilde{\Gamma}_{n-1,k} \neq 0$, which adds a further

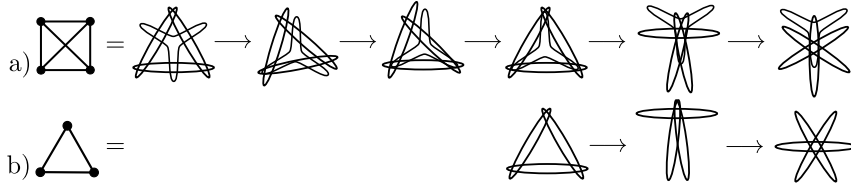


Fig. 2. Two RH-diagrams and their corresponding representations as intersection networks. a) The particles of the fully f-bonded graph $\tilde{\Gamma}_{4,3}$ generically intersect in six domains, which can be successively contracted down to one. b) The graph $\tilde{\Gamma}_{3,1}$ of the third virial cluster has three intersection centers, which can be shifted together into one domain.

node to the graph, linked by f-bonds to all $n - 1$ nodes. Thus, each RH-diagram is an element of exactly one class

$$\tilde{\Lambda}_{n_0,k} = \bigcup_{m=0}^{\infty} \pi^m(\tilde{\Gamma}_{n_0,k}), \quad (14)$$

with the lowest subgraph $\tilde{\Gamma}_{n_0,k'} \subseteq \tilde{\Gamma}_{n,k}$ uniquely defined by $\pi^{-1}(\tilde{\Gamma}_{n_0,k'}) = 0$. One example has already occurred in the discussion of the Rosenfeld functional. Starting from the single node diagram $\tilde{\Gamma}_{1,1}$, each of the exclusively f-bonded diagrams is then an element of $\tilde{\Lambda}_{1,1}$. An important property of a class of RH-diagrams is that their intersection networks can be chosen to coincide:

Lemma 1 *The intersection network of the class $\tilde{\Lambda}_{n_0,k}$ is defined by its lowest subgraph.*

This is readily seen using a graphical argument. As can be seen from Fig. 1 and Fig. 2, for a given diagram $\tilde{\Gamma}_{n,k}$ there are two types of nodes, those exclusively linked by f-bonds and those belonging to the lowest subdiagram, or “backbone”, $\tilde{\Gamma}_{n_0,k'}$. Choose a specific intersection network for this subgraph. Any further particle can then be attached to this network by overlapping it with all of the previous intersection centers, thus keeping the number of centers unchanged.

Focusing again on the Rosenfeld functional, the first element of the class $\tilde{\Lambda}_{1,1}$ with a non-trivial intersection center is $\tilde{\Gamma}_{2,1}$. Thus all RH-graphs with the second virial diagram as its subgraph can be reduced to an intersecting network whose particles overlap in exactly one center. However, one might also choose $\tilde{\Gamma}_{3,1}$ as the leading element. Then, the sum over all RH-integrals of the class $\tilde{\Lambda}_{3,1}$, contracted to three intersection centers, yields Φ_3 . Thus, once a lowest subgraph and its intersection pattern has been selected, its functional is uniquely fixed by its corresponding class. This solves the first of the previously stated four problems.

As the representation of the functional has been shifted from Mayer- to RH-diagrams, it is also necessary to rewrite the functional itself (4) in this new basis. This transformation has already been shown by Ree and Hoover to be a linear combination, weighted by the sign of f-numbers [25, 13]:

$$\tilde{\Gamma}_{n,k} = \sum_{k'}^{\tilde{\Gamma}_{n,k} \subseteq \Gamma_{n,k'}} \Gamma_{n,k'} \quad , \quad \Gamma_{n,k} = \sum_{k'}^{\Gamma_{n,k} \subseteq \tilde{\Gamma}_{n,k'}} (-1)^{|\Gamma_{n,k}| - |\tilde{\Gamma}_{n,k'}|} \tilde{\Gamma}_{n,k'} \quad . \quad (15)$$

When inserted into the sum of Mayer clusters of n vertices (5), the summation order can be exchanged

$$\Gamma_n = \sum_{k'} \Gamma_{n,k'} = \sum_{k'} \sum_{\substack{\Gamma_{n,k'} \subseteq \tilde{\Gamma}_{n,k}}} (-1)^{|\Gamma_{n,k'}| - |\tilde{\Gamma}_{n,k}|} \tilde{\Gamma}_{n,k} = \sum_k a_{n,k} \tilde{\Gamma}_{n,k}, \quad (16)$$

leading to the “star-content” of a RH-graph [25]:

$$a_{n,k} = \sum_{k'} \sum_{\substack{\Gamma_{n,k'} \subseteq \tilde{\Gamma}_{n,k}}} (-1)^{|\Gamma_{n,k'}| - |\tilde{\Gamma}_{n,k}|}. \quad (17)$$

An important property of the star-content, proven by Ree and Hoover, is its recursion relation under removal of an exclusively f-bonded vertex point [25]. When the operator π^{-1} from Def. 1 is applied to Γ_n , the sum separates into star-diagrams $\Gamma_{n-1,k'}$ and 1-path connected graphs with articulation points $\Gamma_{n-1,t}^A$, each weighted by their sign of f-numbers in order to avoid overcounting of contributions:

$$\begin{aligned} \pi^{-1}(\Gamma_n) &= \sum_k \sum_{k'}^{\Gamma_{n-1,k'} \subset \Gamma_{n,k}} (-1)^{|\Gamma_{n,k}| - |\Gamma_{n-1,k'}|} \Gamma_{n-1,k'} \\ &\quad + \sum_k \sum_t^{\Gamma_{n-1,t}^A \subset \Gamma_{n,k}} (-1)^{|\Gamma_{n,k}| - |\Gamma_{n-1,t}^A|} \Gamma_{n-1,t}^A. \end{aligned} \quad (18)$$

Focusing on the first part, the order of summation can be exchanged, resulting in a sum over those $\Gamma_{n,k}$ -graphs, which lead to the same $\Gamma_{n-1,k'}$ diagram after removing a node. If this node is linked by m bonds, these bonds can be distributed in $(n-1)!/(m!(n-m)!)$ ways among the residual $n-1$ vertex points, each weighted by a sign-factor of $(-1)^m$. The first sum therefore simplifies to:

$$\begin{aligned} \sum_{k'} \sum_k^{\Gamma_{n,k} \supset \Gamma_{n-1,k'}} (-1)^{|\Gamma_{n,k}| - |\Gamma_{n-1,k'}|} \Gamma_{n-1,k'} &= \sum_{k'} \sum_{m=2}^{n-1} \binom{n-1}{m} (-1)^m \Gamma_{n-1,k'} \\ &= (n-2) \Gamma_{n-1}. \end{aligned} \quad (19)$$

The second part is a sum over $\Gamma_{n,k}$ and its 1-path connected subgraphs $\Gamma_{n-1,t}^A$. Again, the order of summation can be exchanged, resulting in a weighted sum over all permutations of $0 \leq m \leq n-1$ bonds linked to the residual $n-1$ nodes. In order to perform this sum, observe that a 1-path connected diagram is a linear chain of star-graphs, connected by articulation points, here indicated by \ast' :

$$\Gamma_{n-1,t}^A = \Gamma_{n_1,k_1} \ast \Gamma_{n_2,k_2} \ast \dots \ast \Gamma_{n_p,k_p}, \quad (20)$$

with $n-1 = n_1 + n_2 + \dots + n_p$ nodes. Any partition of m bonds between the vertex P_n , which is to be removed from $\tilde{\Gamma}_{n,k}$, and the non-articulation points can now be compensated by a copy of this same diagram with an additional bond between P_n and one of the articulation points. Having the same subgraph but differing by one f-bond, the two diagrams cancel each other in Eq. (18). The sum therefore decouples into the partition of bonds on non-articulation vertices and articulation ones. The flanking graphs Γ_{n_1,k_1} ,

Γ_{n_p, k_p} are each joined by one articulation point, while the center ones carry two. Their individual contributions to the weighted sum are therefore

$$\sum_{m=0}^{n_i-2} \binom{n_i-2}{m} (-1)^m = 0, \quad \sum_{m=1}^{n_i-1} \binom{n_i-1}{m} (-1)^m = -1 \quad (21)$$

yielding an overall factor of $(-1)^2 = 1$ and leaving a sum over all permutations of bonds between the articulation points and P_n :

$$\sum_t \sum_k^{\Gamma_{n,k} \supset \Gamma_{n-1,t}} (-1)^{|\Gamma_{n,k}| - |\Gamma_{n-1,t}|} \Gamma_{n-1,t} = \sum_k \sum_{m=0}^{p-1} \binom{p-1}{m} (-1)^m \Gamma_{n-1,t} = 0. \quad (22)$$

Combining the two results (19), (22), the total sum of (18) reduces to the recursion relation of Ree and Hoover [25]:

$$\pi^{-1}(\Gamma_n) = (n-2) \Gamma_{n-1}. \quad (23)$$

An analogous relation can be derived for RH-diagrams, inserting the recursion relation into (16) and observing that π^{-1} removes $n-1$ f-bonds from a RH-diagram $\tilde{\Gamma}_{n,k}$:

$$\begin{aligned} \pi^{-1}(\Gamma_n) &= \sum_k \pi^{-1}(a_{n,k} \tilde{\Gamma}_{n,k}) = (-1)^{n-1} \sum_k a_{n,k} \tilde{\Gamma}_{n-1,k} \\ &= (n-2) \Gamma_{n-1} = (n-2) \sum_{k'} a_{n-1,k'} \tilde{\Gamma}_{n-1,k'}. \end{aligned} \quad (24)$$

Comparing terms, the resulting recursion relation is again independent of k :

$$a_{n,k} = (-1)^{n-1} (n-2) a_{n-1,k'} \quad (25)$$

and by repeated application yields the star-content [25]:

$$a_{n,k} = (-1)^{\binom{n}{2} - \binom{m}{2}} \frac{(n-2)!}{(m-2)!} a_{m,k'}. \quad (26)$$

Thus, once it has been calculated for the lowest diagram of a class $\tilde{\Lambda}_{n_0,k}$, the coefficients for all further graphs are known.

So far, we have focused on labeled graphs, ignoring that the physical particles in the partition function are indistinguishable. Transferring to unlabeled RH-diagrams therefore introduces an additional sum over all inequivalent permutations of the labels on the vertex points. For its derivation the e-bonds can be ignored, as they do not change the graph's symmetry, yielding the "symmetry factor" $\sigma_{n,k}$ already known from Mayer clusters. In combination with the star-content, we define the combinatorial prefactor of the virial clusters in RH-graphs:

$$\tilde{\sigma}_{n,k} = -\frac{1}{n!} \sigma_{n,k} a_{n,k}, \quad (27)$$

where the additional factor $1/n!$ has been inserted for later convenience. The last step in proving the resummability of cluster integrals for a given class $\tilde{\Lambda}_{n_0,k}$ therefore requires the derivation of a recursion relation for $\sigma_{n,k}$.

The symmetry factor counts the number of inequivalent labelings of a RH- or Mayer graph $\Gamma_{n,k}$ under the permutation group S_n . Its group elements operate on the product of

f-functions, which define a representation space by $\lambda : \Gamma_{n,k} \rightarrow \text{prod}(f_{ij})$ and are symmetric under exchange of positions and indices:

$$\gamma := \{f_{ij} = f_{ji}, f_{ij}f_{kl} = f_{kl}f_{ij}\}, \quad \gamma\lambda(\Gamma_{n,k}) = \lambda(\Gamma_{n,k}). \quad (28)$$

The group of equivalent labelings is then the automorphism group of its diagram and a subset of the symmetric group S_n

$$\text{Aut}(\Gamma_{n,k}) = \{g \in S_n \mid g\lambda(\Gamma_{n,k}) = \gamma\lambda(\Gamma_{n,k})\} \quad (29)$$

subject to the invariance relation $\gamma^{-1} \circ g = \text{id}$. Correspondingly, the set of inequivalent labelings is generated by the coset $S_n/\text{Aut}(\Gamma_{n,k})$, whose number of elements is the symmetry factor of the graph

$$\sigma_{n,k} = \frac{|S_n|}{|\text{Aut}(\Gamma_{n,k})|}. \quad (30)$$

An extensive list of Mayer diagrams and their automorphism groups has been tabulated by Uhlenbeck and Riddell [46, 29].

In generally, determining the automorphism group of a given graph is non-trivial. However, if it is known for the lowest element of a class $\tilde{\Lambda}_{n_0,k}$, the groups of all further diagrams are known:

Lemma 2 *Let $\tilde{\Gamma}_{n,k} \in \tilde{\Lambda}_{n_0,k}$ with lowest element $\tilde{\Gamma}_{n_0,k}$. Its automorphism group then factorizes into the direct product:*

$$\text{Aut}(\tilde{\Gamma}_{n,k}) = S_{n-n_0} \times \text{Aut}(\tilde{\Gamma}_{n_0,k}). \quad (31)$$

The proof is as follows: Because $\tilde{\Gamma}_{n_0,k}$ is the lowest element of the class, $\pi^{-1}\tilde{\Gamma}_{n_0,k} = 0$, each vertex is connected to at least one e-bond, whereas the remaining $n - n_0$ nodes are only linked by f-bonds. Shifting an f-bonded label to a vertex with an e-bond would therefore result in an inequivalently labeled diagram. Thus, f-bonded nodes can only be permuted under themselves by S_{n-n_0} , completing the proof.

With the recursion relation for the star content (26) and the dimension of the automorphism group

$$|\text{Aut}(\tilde{\Gamma}_{n,k})| = (n - n_0)! |\text{Aut}(\tilde{\Gamma}_{n_0,k})|, \quad (32)$$

the RH-diagrams of a given class have the symmetry factor:

Lemma 3 *Let $\tilde{\Gamma}_{n,k}$ be an element of the class $\tilde{\Lambda}_{n_0,k}$ of RH-graphs with lowest element $\tilde{\Gamma}_{n_0,k}$. Its symmetry factor is:*

$$\begin{aligned} \tilde{\sigma}_{n,k} &= -(-1)^{\binom{n}{2} - \binom{n_0}{2}} \binom{n-2}{n_0-2} \frac{a_{n_0,k}}{|\text{Aut}(\tilde{\Gamma}_{n_0,k})|} : & n_0 \geq 3 \\ \tilde{\sigma}_{n,k} &= (-1)^{\binom{n}{2}} \frac{1}{n(n-1)} : & n_0 = 1 \end{aligned} \quad (33)$$

The case $n_0 \geq 3$ follows from the previous calculations. But $n_0 = 1$ and $n_0 = 2$ have to be considered separately, because the recursion relation (26) only applies to $n_0 \geq 2$, while (31) requires $\tilde{\Gamma}_{n_0,k}$ to be the lowest element of the class. Observing that $\tilde{\Gamma}_{1,1} = \pi^{-1}(\tilde{\Gamma}_{2,1})$ and $a_{2,1} = a_{1,1} = 1$ closes the proof.

It is instructive to derive the symmetry factors for the diagrams of Fig. 1. $\tilde{\Gamma}_{4,3}$ is a fully f-bonded graph and therefore belongs to $\tilde{\Lambda}_{1,1}$, already covered by (33). The next diagram $\tilde{\Gamma}_{4,2}$ has star-content $a_{4,2}(|) = 0$. Thus, all graphs with a single e-bond drop out of the virial series $\tilde{\sigma}_n(|) = 0$. Actually, the same applies to roughly half of the RH-diagrams, improving the convergence of the virial expansion. The final example $\tilde{\Gamma}_{4,1}$ has two separate e-bonds, star-content $a_{4,1}(|) = 1$, and cyclic permutation symmetry $\text{Aut}(\tilde{\Gamma}_{4,1}) = \mathbb{Z}_4 \times \mathbb{Z}_2$. The prefactors of all related graphs are therefore

$$\tilde{\sigma}_n(|) = (-1)^{\binom{n}{2}} \frac{1}{16} (n-2)(n-3). \quad (34)$$

Eq. (33) solves the second of the four problems stated at the beginning of this section and also holds the solution to the fourth one. As has been shown before in 3 dimensions [16], the intersection probability of a network of overlapping particles decouples into a convolute of curvature forms $K_n(r_a)$ for each intersection center with n particles. This observation is sufficient to write down a generic functional for a given intersection network and RH-class:

Theorem 1 *Let $\tilde{\Gamma}_{n_0,k}$ be the lowest element of the class $\tilde{\Lambda}_{n_0,k}$. The free-energy functional density of a network with $p \geq 1$ intersection centers is then determined by*

$$\Phi_1(\tilde{\Gamma}_{1,1}|r_a) = \sum_{n \geq 2} \frac{1}{n(n-1)} \int K_n(r_a, \{\gamma_i\}) \rho(\gamma_1) \dots \rho(\gamma_n) d\gamma_1 \dots d\gamma_n \quad (35)$$

for $n_0 = 1$, while higher order functionals for $n_0 > 3$, are derived by

$$\begin{aligned} \Phi_p(\tilde{\Gamma}_{n_0,k}|r_{a_1}, \dots, r_{a_p}) &= -(-1)^{\binom{n_0}{2}} \frac{a_{n_0,k}}{|\text{Aut}(\tilde{\Gamma}_{n_0,k})|} \sum_{n \geq n_0} \binom{n-2}{n_0-2} \\ &\times \int K_{n_1}(r_{a_1}, \{\gamma_{i_1}\}) \dots K_{n_p}(r_{a_p}, \{\gamma_{i_p}\}) \rho(\gamma_1) \dots \rho(\gamma_n) d\gamma_1 \dots d\gamma_n \end{aligned} \quad (36)$$

with the integral kernel $K_{n_j}(r_a, \{\gamma_i\})$ determining the intersection probability of n_j particles which intersect in r_a and with particle positions γ_i for $i = 1, \dots, n_j$.

The first half of the proof determines the numerical prefactor, combining the symmetry factor of (33) and the sign of f-bonds $(-1)^{|\tilde{\Gamma}_{n,k}|}$, which is not accounted for by the intersection forms. It partially cancels with the sign of $\tilde{\sigma}_{n,k}$ using

$$|\tilde{\Gamma}_{n,k}| = |\tilde{\Gamma}_{n_0,k}| + \binom{n}{2} - \binom{n_0}{2}, \quad (37)$$

leaving a constant only depending on the lowest element of $\tilde{\Lambda}_{n_0,k}$ and an n -dependent binomial coefficient. The second half of the proof deals with the factorization of the intersection probability into integral kernels, which will be the topic of the next section. There it will also be shown, how to generalize the functionals to e-bonds and mixtures of particles.

3. Intersection Probability in N Dimensions

In this section we complete the proof of Theorem 1, determining the intersection probability for networks of overlapping particles. First, the basic ideas of integral geometry are summarized, determining the intersection probability of clusters of particles with one intersection center and then generalized to networks of clusters.

Integral geometry determines the intersection probability between manifolds under translations and rotations with respect to their imbedding space. It has a long history [39, 43], but its modern representation has been founded by Blaschke and Santalo, and further generalized by Chern to n dimensions using differential forms [2, 3, 4]. Chern also explained the connection between the kinematic measure and the Euler form, determining the Blaschke-Santalo-Chern equation for two intersecting manifolds [2, 39]. Up to a sign, this result coincides with Rosenfeld's decoupling of the second virial integral (7). Using this approach, we calculated the intersection probability for an arbitrary set of particles overlapping in a common domain, rederiving the Rosenfeld functional for 3 dimensions. This calculation will be simplified in the following and extended to arbitrary dimension n .

For now, let Σ_k be a set of identical, $n - 1$ dimensional, smooth, orientable, compact, boundary free, Riemannian manifolds with particle index $k = 1, \dots, N$, imbedded into $D_k : \Sigma_k \hookrightarrow \mathbb{R}^n$. For physical reasons we will further assume that the particles D_k only have cavities that are accessible to all other particles. Each domain is then covered by coordinate patches with an orthonormal, positively oriented coordinate frame $(\hat{e}_1^{(k)}, \dots, \hat{e}_n^{(k)})$ at each point $p \in D_k$, with the normal vector $\hat{e}_n^{(k)}$ pointing into the outside direction of the surface $\Sigma_k = \partial D_k$. Being a differential manifold, the geometry of Σ and D are represented by vielbein and connection forms

$$\theta_i = \hat{e}_i dp, \quad \omega_{ij} = \hat{e}_i d\hat{e}_j \quad \text{for } i, j = 1, \dots, n, \quad (38)$$

and the intrinsic forms of torsion and curvature

$$T_i = d\theta_i - \omega_{ij} \wedge \theta_j, \quad \Omega_{ij} = d\omega_{ij} - \omega_{ik} \wedge \omega_{kj}, \quad (39)$$

with the torsion $T_i = 0$ vanishing for a Riemannian manifold. Here and in the following we implicitly assume a sum over pairs of identical indices. Coordinate frames of different patches are connected by $g_{ij} \in \text{SO}(n)$, transforming vectors $e'_i = g_{ij} e_j$ and differential forms

$$\theta'_i = g_{ij} \theta_j, \quad \omega'_{ij} = g_{ik}^{-1} \omega_{kl} g_{lj} + g_{ik}^{-1} dg_{kj}, \quad \Omega'_{ij} = g_{ik}^{-1} \Omega_{kl} g_{lj}. \quad (40)$$

Each Riemannian manifold also defines a semisimple group [10], which for the imbedding space \mathbb{R}^n is the isometric or Euclidean group $\text{ISO}(n) = \text{SO}(n) \ltimes \mathbb{R}^n$. Its Lie algebra $\text{iso}(n)$ has a representation in the vielbein and connection forms generating translations and rotations

$$\begin{pmatrix} \omega_{ij} & \theta_i \\ -\theta_j & 0 \end{pmatrix} \in \text{iso}(n) \quad (41)$$

and whose volume form, or Haar measure, is the “kinematic measure”

$$K(\mathbb{R}^n) = \bigwedge_{1 \leq i < j \leq n} \omega_{ij} \bigwedge_{1 \leq i \leq n} \theta_i. \quad (42)$$

An alternative interpretation uses the representation as a chain of cosets

$$\text{SO}(k)/\text{SO}(k-1) = S^{k-1}, \quad \text{vol}(S^{k-1}) = 2\pi^{k/2}/\Gamma(k/2), \quad (43)$$

which allows to rewrite products of connection forms into integral measures of spheres

$$dS^{k-1} = \omega_{1,k} \wedge \dots \wedge \omega_{k-1,k}. \quad (44)$$

With a particle D imbedded, the vector space of \mathbb{R}^n splits into the tangential $T\Sigma$ and normal space $N\Sigma$ along with a similar decoupling of the rotation group into $SO(n-1)$ and the coset $SO(n)/SO(n-1)$. The kinematic measure (42) separates correspondingly into the three parts

$$K(\partial D) = \bigwedge_{\alpha=1}^{n-1} \omega_{\alpha n} \bigwedge_{i=1}^n \theta_i \wedge d\text{vol}(SO(n-1)) \quad (45)$$

of the curvature (also Euler or highest Chern-Simons) form, the measure of translations, and the volume form of $SO(n-1)$.

This result readily generalizes to two and more overlapping domains which intersect in at least a common point. Introducing the notation for identical particles

$$\Sigma^{k_1} \cap D^{k_2} := \underbrace{\Sigma \cap \dots \cap \Sigma}_{k_1\text{-fold}} \cap \underbrace{D \cap \dots \cap D}_{k_2\text{-fold}}, \quad (46)$$

the intersection D^m is again a n dimensional subset of \mathbb{R}^n and therefore applies to the reduced form of the kinematic measure (45). When inserted, $K(\partial D^m)$, the boundary of the intersection domain can be expanded in the series

$$\partial D^m = \sum_{1 \leq k \leq m} \binom{m}{k} \Sigma^k \cap D^{m-k}, \quad (47)$$

setting all terms Σ^k of $k \geq n+1$ to zero. This restriction of the sum is a useful consequence of the following rules of K :

Lemma 4 *Let D be a domain in \mathbb{R}^n with hypersurface Σ . The kinematic measure K of intersecting manifolds then has the properties:*

$$K(a_1 \Sigma_1 + a_2 \Sigma_2) = a_1 K(\Sigma_1) + a_2 K(\Sigma_2) \quad (48)$$

$$K(\Sigma^{k_1} \cap D^{k_2}) = K(\Sigma^{k_1}) \wedge K(D)^{k_2} \quad (49)$$

$$K(\Sigma_1 \cap \Sigma_2) = K(\Sigma_2 \cap \Sigma_1) \quad (50)$$

$$K(\Sigma^k) = 0 \quad \text{for } k \geq n+1 \quad (51)$$

for $\Sigma_1 \cap \Sigma_2 = 0$ and the constants $a_1, a_2 \in \mathbb{N}$:

The proof is as follows: By construction, the differential form (42) is a locally defined probability measure, which decouples for $\Sigma_1 \cap \Sigma_2 = 0$, thus showing (48). The second identity follows from the observation that the kinematic measure of a point $\text{pt} \in \mathbb{R}^n$ moving in the domain D is trivial $K(\text{pt} \cap D) = K(D)$. Setting $\text{pt} \in \Sigma^{k_1} \cap D^{k_2-1}$ then proves (49) by iteration. While the local measure and set theoretic relation $\Sigma_1 \cap \Sigma_2 = \Sigma_2 \cap \Sigma_1$ explains (50). The last equation (51), which justifies the finite sum (47), implies that the intersection probability between a point $\text{pt} \in \Sigma^n$ and a hypersurface Σ is of measure zero. This follows from K being defined on the tangential space of Σ^k , spanned by the normal and tangential vectors $(\hat{e}_1, \dots, \hat{e}_{n-k}, \hat{e}_n^{(1)}, \dots, \hat{e}_n^{(k)})$, proving that the coordinate basis is not defined for $k \geq n+1$ and therefore vanishes for dimensional reasons.

Applying these rules to the boundary of intersections (47), yields the sum

$$K(\partial D^m) = \sum_{1 \leq k \leq m}^{k \leq n} \binom{m}{k} K(\Sigma^k) \wedge K(D)^{m-k}, \quad (52)$$

with $K(D)$ and the curvature forms $K(\Sigma^k)$ decoupled. For $m = 1$ this reproduces (45). But to derive the remaining differential forms we need an explicit representation of the orthonormal and positively oriented vector field at Σ^k . For simplicity, let us define a fixed ordering of surfaces $\Sigma_1 \cap \dots \cap \Sigma_k$. The vector

$$(\hat{e}_1, \dots, \hat{e}_{n-k}, \hat{e}_n^{(1)}, \dots, \hat{e}_n^{(k)}) \in TD^k \quad (53)$$

then defines a coordinate frame at the intersection, spanned by the k outward pointing normal vectors and the $n - k$ tangential directions which can be chosen by (40) to coincide with all surfaces. However, this frame is neither orthonormal nor positively orientated.

The Gram-Schmidt transformation turns this vector frame into an orthonormal basis

$$v_A = \begin{cases} B_{ab} e_n^{(b)} & \text{for } a, b = 1, \dots, k \\ e_\alpha & \text{for } \alpha = 1, \dots, n - k \end{cases} \quad (54)$$

whose upper triangular matrix $B_{ab} \in \text{Gl}(k, \mathbb{R})$ combines into the general coordinate mapping:

$$B_{AB} = \begin{pmatrix} B_{ab} & 0 \\ 0 & 1_{\alpha\beta} \end{pmatrix}. \quad (55)$$

The coordinate frames of individual surfaces are now related by a rotation of the normal vectors

$$\eta_A = \begin{cases} G_{ab} v_b & \text{for } a, b = 1, \dots, k \\ v_\alpha & \text{for } \alpha = 1, \dots, n - k \end{cases} \quad (56)$$

generated by $G_{ab} \in \text{SO}(k, \mathbb{R})$ and extended to the matrix representation

$$G_{AB} = \begin{pmatrix} G_{ab} & 0 \\ 0 & 1_{\alpha\beta} \end{pmatrix}. \quad (57)$$

Combining both transformations, the connection forms $\eta_{AB} = \eta_A d\eta_B$ at an intersection point can be written in the basis of the tangential $\omega_{\alpha\beta}$ and normal directions $\omega_{\beta n}^{(a)}$ of the coordinate frames of Σ_a keeping the normal vector $de_n^{(a)} = 0$ constant

$$\eta_{AB} = \begin{cases} \eta_{ab} = G_{ac}^{-1} dG_{cb} \\ \eta_{a\beta} = G_{ab} B_{bc} \omega_{\beta n}^{(c)} \\ \eta_{\alpha\beta} = \omega_{\alpha\beta} \end{cases}. \quad (58)$$

The curvature form, which generalizes (45) to the intersection space Σ^k , is the product of connection forms with one axial direction fixed. Let us choose η_k as the new normal vector, leaving G_{ak} to be an element of the coset space $\text{SO}(k)/\text{SO}(k-1) = S^{k-1}$

$$\begin{aligned} \bigwedge_{\beta=1}^{n-k} \eta_{\beta k} \bigwedge_{a=1}^{k-1} \eta_{ak} &= \left(\bigwedge_{\beta=1}^{n-k} G_{ka} B_{ab} \omega_{\beta n}^{(b)} \right) \left(\bigwedge_{a=1}^{k-1} G_{ab}^{-1} dG_{bk} \right) \\ &= \text{Pf}_{1, \dots, k}^{n-k}(GB\omega) \wedge d\text{vol}_G(S^{k-1}), \end{aligned} \quad (59)$$

introducing the notation $\text{Pf}_{1,\dots,k}^{n-k}$ for the Pfaffian of an $n-k$ -form of the ordered set of surfaces $\Sigma_1 \cap \dots \cap \Sigma_k$.

In the derivation of (59) we ignored the orientation of the coordinate frame of $T\Sigma^k$ which is not fixed by the Gram-Schmidt process. However, changing the orientation, e.g. by permuting the order of the particles in (54), changes the sign of (59) by $(-1)^{n-1}$. For n odd, this poses no problem. For n even, however, the orientation of the vector frame is relevant and has to be chosen positively orientated to ensure a positive surface form. This uniquely defines the intersection form K_m introduces in Theorem 1:

Theorem 2 *Let $D_{i_1} \cap \dots \cap D_{i_m}$ be a set of n -dimensional domains overlapping in the common intersection point $r_a \in D^m$ and assigned with a positively orientated coordinate frame. Denote by $|S^{k-1}|$ the volume of the S^{k-1} sphere and by $\Theta(D)$ the step function confining the integral measure to the volume of D . Then, the integral kernel of the functionals (35) and (36) has the form:*

$$K_{i_1 \dots i_m}(r_a, \{\gamma_i\}) = \frac{1}{|S^{n-1}|} \sum_{1 \leq k \leq m}^{k \leq n} \binom{m}{k} \int_{G \in S^{k-1}} \text{Pf}(GB\omega)_{i_1 \dots i_k}^{n-k} \wedge d\text{vol}_G(S^{k-1}) \quad (60)$$

$$\times \Theta(D_{i_{k+1}}) \dots \Theta(D_{i_m}),$$

with an integration over the inner area of the Euler sphere S^{k-1} .

This result follows from inserting the curvature form (59) into the kinematic measure (52) and observing that the vectors r_a are already determined by the coordinates $\{\gamma_i\}$ of the 1-particle densities. The integration over γ_i therefore shifts part of the kinematic measure into the definition of the functionals (35) and (36) and leaves the integral kernel with the step functions $\Theta(D)$ and the differential form $\text{Pf}(GB\omega)^{n-k}$. Finally, the normalization $|S^{n-1}|$ has been added to compensate the volume form introduced by (59).

The curvature form (60) defines the integral kernel for one intersection center. To generalize this result to arbitrary networks of overlapping particles, let us introduce the following notation:

Definition 4 *Networks of intersecting particle domains are represented by products of $\gamma_a^{i_1 \dots i_m}$ for each intersection center $r_a \in D_{i_1} \cap \dots \cap D_{i_m}$ of the intersecting domains D_{i_1}, \dots, D_{i_m} .*

When applied to the third virial cluster, shown in Fig. 2b), the generic diagram $\Gamma_{3,1}$ is an intersection network of pairwise overlapping domains, which can be successively contracted from three centers into networks of two and one

$$\gamma_a^{i_1 i_2} \gamma_b^{j_2 i_3} \gamma_c^{j_1 i_3} \rightarrow \gamma_a^{i_1 i_2 i_3} \gamma_c^{j_1 i_3} \rightarrow \gamma_a^{i_1 i_2 i_3}. \quad (61)$$

While $\Gamma_{4,3}$ has the generic network of six centers, with consecutive contraction into five to one intersection domains, as shown in Fig. 2a)

$$\begin{aligned} \gamma_a^{i_1 i_2} \gamma_b^{j_2 i_3} \gamma_c^{j_3 i_1} \gamma_d^{i_1 i_4} \gamma_e^{j_2 i_4} \gamma_f^{j_3 i_4} &\rightarrow \gamma_a^{i_1 i_2 i_4} \gamma_b^{j_2 i_3} \gamma_c^{j_3 i_1} \gamma_e^{j_2 i_4} \gamma_f^{j_3 i_4} \rightarrow \gamma_a^{i_1 i_2 i_4} \gamma_b^{j_2 i_3 i_4} \gamma_c^{j_3 i_1} \gamma_f^{j_3 i_4} \\ &\rightarrow \gamma_a^{i_1 i_2 i_4} \gamma_b^{j_2 i_3 i_4} \gamma_c^{j_1 i_3 i_4} \rightarrow \gamma_a^{i_1 i_2 i_3 i_4}. \end{aligned} \quad (62)$$

This notation for intersection networks readily translates to the integral kernel:

Lemma 5 Let γ_a^i and γ_b^j denote intersection clusters at centers r_a and r_b with particle indices $i = \{i_1, \dots, i_p\}$ and $j = \{j_1, \dots, j_q\}$. And let $e_{k_1 k_2}$ denote a Boltzmann function with arbitrary particle indices k_1, k_2 . Introducing the notation $K(\gamma_a^{j_1 \dots j_m}) = K_{i_1 \dots i_m}(r_a)$ for the intersection form K , the integral kernel for intersection networks is a linear and multiplicative operator

$$K(\gamma_a^i + \gamma_b^j) = K_i(r_a) + K_j(r_b) \quad (63)$$

$$K(\gamma_a^i \gamma_b^j) = K_i(r_a) K_j(r_b) \quad (64)$$

$$K(\gamma_a^i e_{k_1 k_2}) = K_i(r_a) e_{k_1 k_2} . \quad (65)$$

The first identity (63) is a generalization of (48), while the product structure (64) is a consequence of the properties of f-bonds, whose intersection centers overlap independently. Boltzmann functions, however, do not contribute to the curvature form, but define constraints on the integration domain, justifying (65).

Less trivial, however, is the meaning of the indices. In $\gamma_a^{i_1 \dots i_p}$, each index $i_k \in i$ points to an individual domain D_{i_k} of the $i_k = 1, \dots, N$ particles, while the same index in $K_{i_1 \dots i_p}$ points to the compound $i_k = 1, \dots, M$ represented by the 1-particle density ρ_{i_k} . This change of meaning is a consequence of the thermodynamic limit introduced in Sec. 2.1 and corresponds to the substitution

$$D_k \rightarrow \sum_{i_k=1}^M D_{i_k} \rho_{i_k} . \quad (66)$$

When inserted into the kinematic measure (52), the combinatorial prefactors remain unchanged, while the differential forms are weighted by the density functions. Thus each particle index has to be paired by a corresponding density function:

$$\sum_{i_1, i_2, i_3=1}^M K(\gamma_a^{i_1 i_2} \gamma_b^{i_2 i_3} \gamma_c^{i_3 i_1}) \rho_{i_1} \rho_{i_2} \rho_{i_3} . \quad (67)$$

The generalization to mixtures completes the proof of Theorem 1. And together with the integral kernel (60) and its algebraic structure, we have the necessary tools to systematically derive the density functional for any given class of intersection diagrams. However, to do so efficiently, let us introduce some further notation. First observe that for any k , the curvature form (59) can be written as a volume form

$$\begin{aligned} \text{Pf}(GB\omega)_{i_1 \dots i_k}^{n-k} &= \det(GBh)_{i_1 \dots i_k} \bigwedge_{\alpha=1}^{n-k} \theta_\alpha \\ &= \int_{\mathbb{R}^n} [J \det(GBh)]_{i_1 \dots i_k} \delta(\Sigma_{i_1}) \dots \delta(\Sigma_{i_k}) \bigwedge_{i=1}^n \theta_i , \end{aligned} \quad (68)$$

introducing the curvature matrix $\omega_{\alpha, n} = h_{\alpha\beta} \theta_\beta$ and the delta-function $\delta(\Sigma)$, which projects the integration domain from \mathbb{R}^n to the tangential space of the surface Σ . Correspondingly, products of delta-functions project to the intersection space $\Sigma_{i_1} \cap \dots \cap \Sigma_{i_k}$ associated with the Jacobi determinant

$$J_{i_1 \dots i_k} = \det(\hat{e}_1, \dots, \hat{e}_{n-k}, \hat{e}_n^{(i_1)}, \dots, \hat{e}_n^{(i_k)}) . \quad (69)$$

This transformation allows to factor out the overall volume form and to rewrite the integral kernel (60) as the derivative of a generating function:

Lemma 6 Define the weight functions for $k = 1, \dots, n$ intersecting surfaces

$$w_k^{i_1 \dots i_k} = \frac{1}{|S^{n-1}|} \int_{G \in S^{k-1}} [J \det(GBh)]_{i_1 \dots i_k} d\text{vol}_G(S^{k-1}) \delta(\Sigma_{i_1}) \dots \delta(\Sigma_{i_k}) \quad (70)$$

and the weight function for the domain

$$w_0^{i_1} = \Theta(D_{i_1}) . \quad (71)$$

The integral kernel (60) of the intersection form is then the functional derivative of the product of w_0 -weights:

$$K(\gamma_a^{i_1 \dots i_m}) = \mathcal{D}_a w_0^{i_1}(r_{ai_1}) \dots w_0^{i_m}(r_{ai_m}) , \quad (72)$$

with the derivative on the weight functions at intersection $r_{ai} = r_a - r_i$ defined by

$$\mathcal{D}_a = \sum_{k=1}^n \sum_{i_1 \dots i_k} \frac{1}{k!} w_k^{i_1 \dots i_k}(r_{ai_1}, \dots, r_{ai_k}) \frac{\delta^k}{\delta w_0^{i_1}(r_{ai_1}) \dots \delta w_0^{i_k}(r_{ai_k})} , \quad (73)$$

operating on two and more w_0 -weight functions.

The proof follows by differentiating the integral and significantly simplifies by introducing the extended Kronecker-delta and summation rule:

$$\begin{aligned} \delta_i^j &:= \frac{\delta}{\delta w_0^i(r_{ai})} w_0^j(r_{aj}) , & \sum_j \delta_i^j w_0^j(r_{aj}) &= w_0^i(r_{ai}) , \\ \frac{\delta}{\delta w_0^i(r_{ai})} w_0^j(r_{bj}) &= 0 \quad \text{for } r_a \neq r_b . \end{aligned} \quad (74)$$

Less trivial is the observation that the curvature form (68) and therefore the weight functions are symmetric in the particle indices. This is a consequence of the coupled coordinate system of $T\Sigma^k$, which can be diagonalized using the $\text{SO}(n-k) \times \text{SO}(k)$ invariance of its vector basis. Its explicit calculation gives no further insight and therefore is postponed to App. A.

The derivative (73), which is a consequence of (47), simplifies the construction of a functional in two aspects: first, it hides the sum over the $k = 1, \dots, n$ differential forms in the intersection kernel (60). Second, it leaves the volume weight w_0^i as the only variable in the sums of (35), (36). Thus, each functional is the derivative of a generating function in the virial series of w_0^i . In combination with Theorem 1, this reveals that:

Lemma 7 The virial series of the free-energy functional for a finite number of intersection centers is convergent.

The proof is as follows: It is sufficient to show that the generating function is a convergent series. If γ_0 is the intersection diagram of the lowest element $\tilde{\Gamma}_{n_0, k}$ with p intersection centers. Then, the integral kernel of any higher order element $\pi^m \tilde{\Gamma}_{n_0, k}$ decouples:

$$\int K(\pi^m \gamma_0) \rho^{n_0+m} = (x_{a_1 \dots a_p})^m \int K(\gamma_0) \rho^{n_0} , \quad (75)$$

with the density function defined by

$$x_{a_1 \dots a_p} = \int w_0^i(r_{a_1 i}) \dots w_0^i(r_{a_p i}) \rho_i d\gamma_i . \quad (76)$$

When inserted into the functionals (35), (36), the sum simplifies to a polynomial in x with singularities in $x = 1$ and $x = 0$. However, the virial series is finite in the low-density limit and therefore $x = 0$ a regular point. This leaves $x = 1$ as the only singularity. At thermodynamic equilibrium and with all intersection centers collapsed into a single point, the packing fraction approaches $\eta = 1$, proving that the functional is convergent for $\eta < 1$.

This final result proves the resummability of the approximate density functional and solves the last of the four problems presented at the beginning of Sec. 2.2.

4. The Rosenfeld Functional and Beyond

This last section presents four examples, which provide some insight into the construction of functionals. We begin with the integral kernel for 3 dimensions and derive the functional with one intersection center. It is then shown that Rosenfeld's result is an approximation for almost perpendicular normal vectors. The remaining examples then focus on the functionals with two, three, and four intersection centers.

Starting point for the construction of any functional is the derivation of the integral kernel. This has to be done once for any dimension and is independent of the particle geometry or boundary conditions. For $n = 3$ dimensions, there exists three differential forms:

The case $k = 1$ is elementary. With $G = B = 1$ and assuming a positively oriented orthonormal coordinate frame, the Pfaffian reduces to the Euler form $\text{Pf}_{i_1}^2(GB\omega) = \omega_{13}^{(i_1)} \wedge \omega_{23}^{(i_1)}$ and a trivial integral over the S^0 -sphere

$$\int \text{Pf}_{i_1}^2(GB\omega) \wedge d\text{vol}(S^0) = \omega_{13}^{(i_1)} \wedge \omega_{23}^{(i_1)}. \quad (77)$$

For $k = 2$, the Gram-Schmidt scheme and $\text{SO}(2)$ rotation have the matrix representation:

$$B = \begin{pmatrix} 1 & 0 & 0 \\ -\frac{\cos(\phi_{i_1 i_2})}{\sin(\phi_{i_1 i_2})} & 1 & 0 \\ 0 & 0 & 1 \end{pmatrix}, \quad G = \begin{pmatrix} \cos(\alpha) & \sin(\alpha) & 0 \\ -\sin(\alpha) & \cos(\alpha) & 0 \\ 0 & 0 & 1 \end{pmatrix} \quad (78)$$

$$\phi_{i_1 i_2} = \arccos(\hat{e}_3^{(i_1)} \hat{e}_3^{(i_2)}) \quad , \quad 0 \leq \alpha \leq \phi_{i_1 i_2} \leq 2\pi,$$

depending on the intersection angle $\phi_{i_1 i_2}$. The associate Pfaffian yields the 1-form:

$$\text{Pf}_{i_1 i_2}^1(GB\omega) = \left[\cos(\alpha) - \frac{\cos(\phi_{i_1 i_2})}{\sin(\phi_{i_1 i_2})} \sin(\alpha) \right] \omega_{13}^{(i_1)} + \frac{1}{\sin(\phi_{i_1 i_2})} \sin(\alpha) \omega_{13}^{(i_2)} \quad (79)$$

whose integral over $\alpha \in S^1$ simplifies to

$$\int_{\alpha \in S^1} \text{Pf}_{i_1 i_2}^1(GB\omega) \wedge d\text{vol}_\alpha(S^1) = \frac{1 - \cos(\phi_{i_1 i_2})}{\sin(\phi_{i_1 i_2})} [\omega_{13}^{(i_1)} + \omega_{13}^{(i_2)}]. \quad (80)$$

Finally, for $k = 3$ the integral over the curvature form (59) reduces to the area of the spherical triangle $\Delta \subseteq S^2$

$$\int_{G \in S^2} \text{Pf}_{i_1 i_2 i_3}^0(GB\omega) \wedge d\text{vol}_G(S^2) = \text{area}(\Delta \subseteq S^2) = 2\pi - \phi_{i_2 i_3}^{i_1} - \phi_{i_1 i_3}^{i_2} - \phi_{i_1 i_2}^{i_3} \quad (81)$$

whose value is determined by the Euler or dihedral angles $\phi_{i_1 i_2}^{i_3}$ [11]:

$$\phi_{i_2 i_3}^{i_1} = \arccos(\hat{E}_{i_2} \hat{E}_{i_3}), \quad \hat{E}_{i_1} = \frac{\hat{e}_3^{(i_2)} \times \hat{e}_3^{(i_3)}}{|\hat{e}_3^{(i_2)} \times \hat{e}_3^{(i_3)}|}. \quad (82)$$

Comparing these results to the definition (70) and taking into account the permutation symmetry in the particle indices, we obtain the three weight functions:

$$\begin{aligned} w_1^{i_1} &= \frac{1}{4\pi} \det(h^{(i_1)}) \delta(\Sigma_{i_1}), \quad w_2^{i_1 i_2} = \frac{1}{2\pi} \frac{1 - \cos(\phi_{i_1 i_2})}{\sin(\phi_{i_1 i_2})} [Jh_{12}]^{(i_1)} \delta(\Sigma_{i_1}) \delta(\Sigma_{i_2}) \\ w_3^{i_1 i_2 i_3} &= \frac{1}{4\pi} (2\pi - 3\phi_{i_2 i_3}^{i_1}) J_{i_1 i_2 i_3} \delta(\Sigma_{i_1}) \delta(\Sigma_{i_2}) \delta(\Sigma_{i_3}). \end{aligned} \quad (83)$$

These agree with the weight function $w_2^{i_1 i_2}$ first derived by Wertheim [47, 48] and rediscovered in [7], while $w_3^{i_1 i_2 i_3}$ first occurred in [18].

Next, we will illustrate the application of the derivative and generating function on the functional restricted to one intersection center $\Phi|_1$. It is therefore of type (35), and the virial series sums up to the generating function in the x -variable (76) of the volume weight:

$$\begin{aligned} \Phi|_1(\tilde{I}_{1,1}, r_a) &= \int \sum_{m=2} \frac{1}{m(m-1)} K(\gamma_a^{i_1 \dots i_m}) \rho_{i_1} \dots \rho_{i_m} d\gamma_{i_1} \dots d\gamma_{i_m} \\ &= \mathcal{D}_a \int \sum_{m=2} \frac{1}{m(m-1)} w_0^{i_1}(r_a) \dots w_0^{i_m}(r_a) \rho_{i_1} \dots \rho_{i_m} d\gamma_{i_1} \dots d\gamma_{i_m} \\ &= \mathcal{D}_a \sum_{m=2} \frac{1}{m(m-1)} x_a^m = \mathcal{D}_a [(1-x_a) \ln(1-x_a) + x_a]. \end{aligned} \quad (84)$$

Introducing the weight density

$$n_k(r_a) = \int w_k^{i_1 \dots i_k}(r_{ai_1}, \dots, r_{ai_k}) \rho_{i_1}(r_{i_1}) \dots \rho_{i_k}(r_{i_k}) d\gamma_{i_1} \dots d\gamma_{i_k}, \quad (85)$$

the derivative of the generating function yields the three terms

$$\Phi|_1(\tilde{I}_{1,1}, r_a) = -n_1 \ln(1-n_0) + \frac{1}{2} \frac{n_2}{1-n_0} + \frac{1}{6} \frac{n_3}{(1-n_0)^2} \quad (86)$$

whose structure is well known from the Rosenfeld functional (13). It is well established that the weight functions (8) derive from a Taylor expansion in the \sin and \cos terms of the intersection angles. This has been shown before for n_2 in [7, 8] and by using differential forms [17]. For n_3 , however, we made an inconvenient choice of coordinates for $\Delta \in S^2$ and give here a clearer argument. A more detailed discussion that also includes the zero-dimensional limit will be presented in [19].

Let us introduce the notation $\hat{e}_i := \hat{e}_n^{(i)}$ for the $i = 1, 2, 3$ normal vectors of $\Sigma_1, \Sigma_2, \Sigma_3$ and $e_{ij} := \hat{e}_i \hat{e}_j$ for their scalar product. Further assume that the three vectors approximately set up an orthonormal basis

$$\hat{e}_1 \approx \hat{e}_2 \times \hat{e}_3. \quad (87)$$

The area of the spherical triangle is then $\Delta \approx \pi/2$ with the Jacobi determinant $J_{123} = \det(\hat{e}_1, \hat{e}_2, \hat{e}_3) \approx 1$ and Euler angles ϕ_{ij}^k close to zero. Thus, expanding the argument of *arccos* up to 5'th order

$$z = \hat{E}_1 \hat{E}_2 = (e_{23}e_{13} - e_{12})(1 + \frac{1}{2}e_{23}^2)(1 + \frac{1}{2}e_{13}^2) + \mathcal{O}(e_{ij}^5), \quad (88)$$

yields the small-angle correction of Δ :

$$\begin{aligned} 2\pi - 3 \arccos(z) &= \frac{\pi}{2} + 3(z + \frac{1}{6}z^3) + \mathcal{O}(z^5) \\ &= \frac{\pi}{2} - 3[e_{12} - e_{23}e_{13} + \frac{1}{2}e_{12}(e_{23}^2 + e_{13}^2) + \frac{1}{6}e_{12}^3] + \mathcal{O}(e_{ij}^4) \end{aligned} \quad (89)$$

where only e_{12}^3 is from order z^3 . Rewritten in the weight densities (8), n_3 is to first order in the Euler angle:

$$n_3 = \frac{\pi}{2} n_{\sigma 0}^3 - 3n_{\sigma 0} n_{\sigma 1}^2 + 3[n_{\sigma 1} n_{\sigma 2} n_{\sigma 1} - n_{\sigma 1} n_{\sigma 2} n_{\sigma 3}] - \frac{1}{2} n_{\sigma 3}^2 n_{\sigma 0} + \mathcal{O}(e_{ij}^4 \rho^3). \quad (90)$$

The second term agrees with the Rosenfeld functional, while the prefactor of the third is 4.5 compared to our 3, which is acceptable given that the terms of (13) have been fitted to numerical data. The fourth term disagrees, but is of lower order. More remarkably, the prefactor of the first term disagrees also. Choosing a different point of reference for the Taylor expansion can set the coefficient of the leading term from $\pi/2$ to 0, but never to 1. Here, Tarazona's term for the 3-particle intersection is a better approximation [45], which also includes additional terms from the third order in z . A more detailed discussion can be found in [19].

Our next example derives the functional for three intersection centers, whose lowest RH-diagram is $\tilde{\Gamma}_{3,1}$, which belongs to the class $\tilde{\Lambda}_{1,1}$. Its intersection diagram is the exact third virial cluster $\gamma_a^{i_1 i_2} \gamma_b^{i_2 i_3} \gamma_c^{i_3 i_1}$ show in Fig. 2b). The next particle added to the triangle diagram has to overlap with all three intersection centers, as illustrated by the fourth figure of Fig. 2a) and represented by $\gamma_a^{i_1 i_2 i_4} \gamma_b^{i_2 i_3 i_4} \gamma_c^{i_3 i_1 i_4}$. Adding more particles includes copies of the last one, corresponding to the intersection pattern

$$\gamma_a^{i_1 i_2 i_4 \dots i_m} \gamma_b^{i_2 i_3 i_4 \dots i_m} \gamma_c^{i_3 i_1 i_4 \dots i_m}. \quad (91)$$

To further simplify the notation, let us define $w_a^i := w_0^i(r_{ai})$ for the volume weight at intersection center r_a and particle position r_i . The functional (35) for the 3-center diagrams then factorizes into weight densities of 2 and 3 centers:

$$\begin{aligned} &\sum_{m=3}^{\infty} \frac{1}{m(m-1)} \int K(\gamma_a^{i_1 i_2 i_4 \dots i_m} \gamma_b^{i_2 i_3 i_4 \dots i_m} \gamma_c^{i_3 i_1 i_4 \dots i_m}) \rho_{i_1} \dots \rho_{i_m} d\gamma_1 \dots d\gamma_m \\ &= \mathcal{D}_a \mathcal{D}_b \mathcal{D}_c \sum_{m=3}^{\infty} \frac{1}{m(m-1)} \int (w_a^{i_1} w_c^{i_1} \rho_{i_1}) (w_a^{i_2} w_b^{i_2} \rho_{i_2}) (w_b^{i_3} w_c^{i_3} \rho_{i_3}) \\ &\quad \times (w_a^{i_4} w_b^{i_4} w_c^{i_4} \rho_{i_4}) \dots (w_a^{i_m} w_b^{i_m} w_c^{i_m} \rho_{i_m}) d\gamma_1 \dots d\gamma_m. \end{aligned} \quad (92)$$

Introducing the x -densities of (76) and adding the second virial, we finally arrive at the functional restricted to three and less intersection centers:

$$\begin{aligned} \Phi|_3(\tilde{\Gamma}_{1,1}, r_a, r_b, r_c) &= \frac{1}{2} \mathcal{D}_a x_a^2 \\ &+ \mathcal{D}_a \mathcal{D}_b \mathcal{D}_c \left[\frac{x_{ab} x_{bc} x_{ac}}{x_{abc}^3} \left((1 - x_{abc}) \ln(1 - x_{abc}) + x_{abc} - \frac{1}{2} x_{abc}^2 \right) \right]. \end{aligned} \quad (93)$$

With three intersection centers, it is exact in the second and third virial order, but also significantly more complex due to additional correlation and autocorrelation functions such as $w_1^{i_4}(r_a) w_1^{i_4}(r_b) w_1^{i_4}(r_c)$, which have been shown by Wertheim to be nontrivial to evaluate [48, 49, 50].

Nevertheless, Lemma 6 is an efficient tool to derive new functionals. To compare different levels of approximation, let us summarize all cases of up to four intersection centers. With one center covered by (84), the next level is the 2-center approximation, beginning with the partially contracted third virial cluster, shown in Fig. 2b). All further intersection diagrams are then of the form:

$$\gamma_a^{i_1 i_2 i_3 \dots i_4 \dots i_m} \gamma_b^{j_2 i_3 \dots i_4 \dots i_m}. \quad (94)$$

The case of three centers has already been covered by (91). This leaves the functional with four intersection centers of the two RH-classes $\tilde{\Gamma}_{4,1}$ and $\tilde{\Gamma}_{4,3}$, while the star-content of $\tilde{\Gamma}_{4,2}$ vanishes. The corresponding intersection graphs are:

$$\begin{aligned} &\gamma_a^{i_1 i_2 \dots i_5 \dots i_m} \gamma_b^{j_2 i_3 \dots i_5 \dots i_m} \gamma_c^{i_3 i_4 \dots i_5 \dots i_m} \gamma_d^{i_1 i_4 \dots i_5 \dots i_m} e_{i_1 i_3} e_{i_2 i_4} \\ &+ \gamma_a^{i_1 i_2} \gamma_b^{j_2 i_3 \dots i_4 \dots i_m} \gamma_c^{i_1 i_3 \dots i_4 \dots i_m} \gamma_d^{j_2 i_4 \dots i_5 \dots i_m}, \end{aligned} \quad (95)$$

with the Boltzmann functions e_{ij} included. Determining their generating functions and adding the lower virial terms, yields the complete list of functionals up to four intersections

$$\begin{aligned} \Phi|_1 &= \mathcal{D}_a [(1 - x_a) \ln(1 - x_a) + x_a] \\ \Phi|_2 &= \frac{1}{2} \mathcal{D}_a x_a^2 + \frac{1}{2} \mathcal{D}_a \mathcal{D}_b \frac{x_a + x_b}{x_{ab}} \left[(1 - x_{ab}) \ln(1 - x_{ab}) + x_{ab} - \frac{1}{2} x_{ab}^2 \right] \\ \Phi|_3 &= \frac{1}{2} \mathcal{D}_a x_a^2 + \mathcal{D}_a \mathcal{D}_b \mathcal{D}_c \frac{x_{ab} x_{bc} x_{ac}}{x_{abc}^3} \left[(1 - x_{abc}) \ln(1 - x_{abc}) + x_{abc} - \frac{1}{2} x_{abc}^2 \right] \\ \Phi|_4 &= \frac{1}{2} \mathcal{D}_a x_a^2 + \frac{1}{6} \mathcal{D}_a \mathcal{D}_b \mathcal{D}_c x_{ab} x_{bc} x_{ac} \\ &+ \mathcal{D}_a \mathcal{D}_b \mathcal{D}_c \mathcal{D}_d \frac{x_{ac} x_{bc} x_{abd}}{x_{bcd}^4} \left[(1 - x_{bcd}) \ln(1 - x_{bcd}) + x_{bcd} - \frac{1}{2} x_{bcd}^2 - \frac{1}{6} x_{bcd}^3 \right] \\ &+ \frac{1}{8} \mathcal{D}_a \mathcal{D}_b \mathcal{D}_c \mathcal{D}_d \frac{y_{ab|cd} y_{ad|bc}}{(1 - x_{abcd})^3}, \end{aligned} \quad (96)$$

where we replaced $x_a \rightarrow (x_a + x_b)/2$ in $\Phi|_2$ to satisfy the diagram's symmetry and introduced the definition of the Boltzmann weighted density

$$y_{ab|cd} = \int (w_a^i w_b^j \rho_i) (w_c^j w_d^j \rho_j) e_{ij} d\gamma_i d\gamma_j. \quad (97)$$

The formalism of Lemma 6 is not restricted to the free energy but applies to any thermodynamic object representable by Mayer or RH-graphs. As a final example, let us consider the leading order of the pair-correlation function g_2 . As has been shown for spheres in [25, 27], the dominating RH-graphs are again the fully f-bonded diagrams with two root points connected by an e-bond. The network with the lowest number of intersection centers is therefore

$$\gamma_a^{j_1 i_3 \dots i_m} \gamma_b^{j_2 i_3 \dots i_m} e_{i_1 i_2}, \quad (98)$$

whose combinatorial prefactors have been shown in [27] to combine to 1. The sum over all diagrams then yields g_2 approximated by two intersection centers

$$g_{i_1 i_2}|_2(r_a, r_b, r_{i_1}, r_{i_2}) = \mathcal{D}_a \mathcal{D}_b \frac{e_{i_1 i_2} w_a^{i_1} w_b^{i_2}}{1 - x_{ab}}, \quad (99)$$

without a sum over the particle indices i_1, i_2 .

The derivation of these examples is a result of simple algebra. But the increasing order of n-point densities gives a first impression of the difficulties one will have to overcome to minimize such functionals. The two centers of $\Phi|_2$ define a rotation axis over which the weight functions can individually be averaged without further constraints. Significantly more difficulties arise from $\Phi|_3$. The three centers form a ring, which cause the positions and orientations of the particles to couple. Still, the integrals can be evaluated by Wertheim's application of the Radon transformation [48]. Finally, $\Phi|_4$ contains the elements of RH-class $\tilde{\Lambda}_{4,1}$, introducing e-bonds and therefore constraints on the particles not to overlap. This adds a further level of complexity to the model, which effectively limits the DFT approach to these four functionals.

5. Discussion and Conclusion

The last examples have shown that the construction of a functional for hard particles is a rather simple task. For a given virial order, one first chooses the intersection network and derives its generating function in the volume density. In a second step, one derives the weight functions from the intersection kernel and finally performs the derivatives. But the non-locality of the problem has not vanished; instead it is hidden in the convolute of the intersection coordinates.

The rapidly increasing complexity with the number of intersection centers effectively imposes an upper bound on the order of the functional to be applied. On the other hand, the long range ordering of the particles in the high density limit also defines a lower bound on the number of intersection centers. This is because the minimization process cannot produce a particle density with a lower symmetry as the invariance group of the functional. The underlying intersection network therefore has to be complex enough to reduce the isometric group of the imbedding space to a sufficiently small subgroup. But here one can be optimistic. The Rosenfeld functional with the highest rotational and translational symmetry already predicts, e.g., the nematic phase. And the next leading order $\Phi|_2$ only depends on 1- and 2-point densities without further geometric constraints due to e-bonds or rings which, e.g., complicates the evaluation of $\Phi|_4$ and $\Phi|_3$.

But it might not be even necessary to go beyond the leading order. As the last example has already indicated, any correlation function can be approximated by intersection

diagrams and represented in weight densities. This will be investigated in a forthcoming paper and applied to couple soft interactions to the hard-particle reference fluid. The soft potential, however, significantly deforms the hard-particle phase structure, so that a detailed knowledge of the hard-particle phase becomes less important.

For the derivation of the functional we made rather strong assumptions about the particles' geometry, demanding their surfaces to be smooth and bounded. Both requirements can be weakened. Actually, it is sufficient for the manifolds to be compact, twice differentiable, and Riemannian or representable by triangulation. And instead of the Euclidean imbedding space it is possible to use complex, projective or hyperbolic spaces, as long as they have infinite volume. Finite volumes can be constructed from them by adding external potentials. These spaces and imbeddings are probably of less physical interest. But it is known from computer simulations that the phase structure of a system depends sensitively on the geometry. Thus, instead of intrinsic objects, such as Chern or Chern-Simons classes, it is possible to characterize manifolds by their many-particle properties. The connection between single- and many-particle properties is the integral kernel, whose derivation closely parallels that of Chern-Simons forms. The virial coefficients of the free-energy expansion therefore contain the integral values of these classes, either obtained by computer simulations, minimizing a functional, or other methods. This allows to identify the numerical value of any virial order with its respective differential forms. Manifolds can then be characterized by these numbers and tested by mixing them with simpler particles such as spheres of different sizes.

The explicitly known dependence of the non-local functional therefore might provide a direct view into the thermodynamics of hard particles that is only rivalled by scalar field theory and the Ising model.

Acknowledgements. The author wishes to thank André Bardow and Kai Leonhard for support of this work as part of his PhD thesis. He also gratefully acknowledges Matthieu Marechal for many helpful discussions and sharing his insight into Ree-Hoover diagrams, also Annett Schwarz and Christian Jens for improving the manuscript.

This work was performed as part of the Cluster of Excellence "Tailor-Made Fuels from Biomass", funded by the Excellence Initiative of the German federal and state governments.

A. Appendix

The current section completes the proof Lemma 6 that the weight functions (70) are symmetric in the particles indices and permuted by $SO(k)$ rotations.

For the surfaces $\Sigma_1, \dots, \Sigma_k$, let us define the k coordinate frames

$$\Sigma_m : \underbrace{(\hat{e}_1^{(m)}, \dots, \hat{e}_{n-m}^{(m)})}_{\text{tangential}}, \underbrace{\hat{e}_{n-m+1}^{(m)}, \dots, \hat{e}_n^{(m)}}_{\text{normal}} \quad \text{for } m = 1, \dots, k \quad (100)$$

and the Pfaffian form (68)

$$\text{Pf}(GB\omega)^{n-k}_{1\dots k} = \det(GBh)_{1\dots k} \bigwedge_{\alpha=1}^{n-k} \theta_{\alpha}^{(1)}. \quad (101)$$

This choice of the vector base defines a specific ordering of the particles' indices $1, \dots, k$, which can be viewed as a nested intersection of surfaces

$$((\Sigma_1 \cap \Sigma_2) \cap \Sigma_3) \cap \Sigma_4 \dots, \quad (102)$$

with Σ_1 as the reference system. It therefore fails the permutation invariance of the intersection probability. However, not the curvature form but the kinematic measure (50) has to be $\text{SO}(n-k) \times \text{SO}(k)$ invariant. We therefore have to prove the permutation symmetry of the integral

$$\begin{aligned} & \int K(\Sigma_1 \cap \dots \cap \Sigma_k) \wedge K(D_2) \wedge \dots \wedge K(D_k) \\ &= \int \det(GBh)_{1\dots k} \bigwedge_{\alpha=1}^{n-k} \theta_{\alpha}^{(1)} \frac{d\text{vol}(\text{SO}(n-k))}{|\text{SO}(n-k)|} \wedge K(D_2) \wedge \dots \wedge K(D_k). \end{aligned} \quad (103)$$

Generalizing Chern's arguments for two intersection surfaces [3, 39], the translational measure of Σ^k has been extended by $\text{SO}(n-k)$ to the kinematic measure of \mathbb{R}^{n-k} . This leaves us to rotate the normal vectors $\hat{e}_n^{(2)}, \dots, \hat{e}_n^{(k)}$ into the tangential direction of Σ_1 . For the nested coordinate frame (102), we can chose the $\text{SO}(m)$ transformations of the "normal" directions to rotate $\hat{e}_n^{(m)}$ into the basis of Σ_1 while keeping the vectors of $\Sigma_2, \dots, \Sigma_{m-1}$ fixed:

$$\Sigma_m \rightarrow \Sigma_1 : \quad \text{SO}(m)/\text{SO}(m-1) = S^{m-1}. \quad (104)$$

Introducing the spherical vector $(x_1^{(m)}, \dots, x_m^{(m)}) \in S^{m-1}$, the normal vector of Σ_m transforms into the basis of Σ_1

$$\hat{e}_n^{(m)} = \sum_{p=1}^m x_p^{(m)} \hat{e}_{n-p+1}^{(1)} \quad \text{for} \quad \sum_{p=1}^m (x_p^{(m)})^2 = 1 \quad (105)$$

and their dual basis forms

$$\begin{aligned} \theta_n^{(m)} &= \sum_{p=2}^m x_p^{(m)} \theta_{n-p+1}^{(1)} = x_m^{(m)} \theta_{n-m+1}^{(1)} + \mathcal{O}(\theta_{\alpha}^{(1)}) \\ &\quad \text{for } n-m+2 \leq \alpha \leq n-1. \end{aligned} \quad (106)$$

Here, the symbol $\mathcal{O}(\theta_{\alpha}^{(1)})$ indicates elements, which drop out when inserted into the skew symmetric product (103) as they already occur at a lower m . This transforms the normal directions into the tangential forms of Σ_1

$$\theta_n^{(2)} \wedge \dots \wedge \theta_n^{(k)} = x_2^{(2)} \dots x_k^{(k)} \theta_{n-1}^{(1)} \wedge \dots \wedge \theta_{n-k+1}^{(1)}, \quad (107)$$

which are complementary to the already existing elements in (103).

The analogous transformation has to be done for the connection forms. Adopting the notation of (100), we separate the forms into two groups

$$\Sigma_m : \quad \underbrace{\omega_{1,n}^{(m)} \wedge \dots \wedge \omega_{n-m,n}^{(m)}}_{\text{tangential}} \wedge \underbrace{\omega_{n-m+1,n}^{(m)} \wedge \dots \wedge \omega_{n-1,n}^{(m)}}_{\text{normal}}. \quad (108)$$

Again, the tangential directions transform by the coset elements of S^{m-1}

$$\begin{aligned} \omega_{\alpha,n}^{(m)} &= x_m^{(m)} \omega_{\alpha,n-m+1}^{(1)} + \mathcal{O}(\omega_{\alpha,\beta}^{(1)}) \\ &\quad \text{for } 1 \leq \alpha \leq n-m, \quad n-m+2 \leq \beta \leq n-1, \end{aligned} \quad (109)$$

whose products provide the complementary part to the $\text{SO}(n-k)$ form of (103)

$$\bigwedge_{m=2}^k \bigwedge_{\alpha=1}^{n-m} \omega_{\alpha,n}^{(m)} = \left[\prod_{m=2}^k (x_m^{(m)})^{n-m} \right] \bigwedge_{m=2}^k \bigwedge_{\alpha=1}^{n-m} \omega_{\alpha,n-m+1}^{(1)}. \quad (110)$$

On the other hand, the normal components of the connection forms (108) transform under the adjoint of $g_{\alpha\beta} \in \text{SO}(m)$

$$\omega_{\alpha,n}^{(m)} = g_{\alpha\beta}^{-1} \hat{e}_\beta^{(1)} d(g_{n\gamma} \hat{e}_\gamma^{(1)}) = g_{\alpha\beta}^{-1} dg_{n\beta} + \mathcal{O}(\omega_{\beta\gamma}^{(1)}) \quad (111)$$

for $n-m+1 \leq \beta < \gamma \leq n-1$

with the coset element $g_{n\alpha} \in \text{SO}(m)/\text{SO}(m-1)$ leaving the normal vectors invariant. Forming their product, they combine into the group measure of $\text{SO}(k)$ modulo further connections

$$\begin{aligned} \bigwedge_{m=2}^k \bigwedge_{\alpha=n-m+1}^{n-1} \omega_{\alpha,n}^{(m)} &= \bigwedge_{m=2}^k [d\text{vol}(S^{m-1}) + \mathcal{O}(\omega_{\beta\gamma}^{(1)})] \\ &= d\text{vol}(\text{SO}(k)) + \mathcal{O}(\omega_{\beta\gamma}^{(1)}). \end{aligned} \quad (112)$$

Finally, inserting the transformed normal components into the kinematic measure (103), yields a differential form which is obviously $\text{SO}(k)$ invariant

$$\begin{aligned} &\int K(\Sigma_1 \cap \dots \cap \Sigma_k) \wedge K(D_2) \wedge \dots \wedge K(D_k) \\ &= \int \frac{\det(GBh)}{|\text{SO}(n-k)|} \prod_{m=2}^k (x_m^{(m)})^{n-m+1} d\text{vol}(\text{SO}(k)) \wedge K(\Sigma_1) \wedge \dots \wedge K(\Sigma_k). \end{aligned} \quad (113)$$

The product of $x_m^{(m)}$ terms is the Jacobian J of the transformation into spherical coordinates and has the parameterization in terms of $\text{SO}(m)$ rotation angles for $m = 1, \dots, k$

$$x_m^{(m)} = \prod_{\alpha=1}^{m-1} \sin(\phi_{\alpha,m}), \quad (114)$$

proving the invariance of the weight functions (70) under $\text{SO}(k)$ -generated permutations of particles indices and thus of Lemma 6.

References

1. Brader, J.M., Esztermann, A., Schmidt, M.: Colloidal rod-sphere mixtures: Fluid-fluid interfaces and the Onsager limit. *Phys. Rev. E* **66**(3), 031,401 (2002)
2. Chern, S.S.: On the kinematic formula in the euclidean space of n dimensions. *Am. J. Math.* **74**, 227–236 (1952)
3. Chern, S.S.: Integral formulas for hypersurfaces in euclidean space and their applications to uniqueness theorems. *Indiana Univ. Math. J.* **8**, 947–955 (1959)
4. Chern, S.S.: On the kinematic formula in integral geometry. *J. Math. Mech.* **16**, 101–118 (1966)
5. Dreizler, R., Gross, E.: *Density Functional Theory*. Springer (1990)
6. Evans, R.: The nature of the liquid-vapour interface and other topics in the statistical mechanics of non-uniform, classical fluids. *Adv. Phys.* **28**, 143–200 (1979)
7. Hansen-Goos, H., Mecke, K.: Fundamental measure theory for inhomogeneous fluids of nonspherical hard particles. *Phys. Rev. Lett.* **102**(1), 018,302 (2009)

8. Hansen-Goos, H., Mecke, K.: Tensorial density functional theory for non-spherical hard-body fluids. *J. Phys.: Condens. Matter* **22**, 364,107 (2010)
9. Hansen-Goos, H., Roth, R.: Density functional theory for hard-sphere mixtures: The white-bear version mark II. *J. Phys.: Condens. Matter* **18**, 8413–8425 (2006)
10. Helgason, S.: *Differential Geometry, Lie Groups, and Symmetric Spaces*. Academic Press (1978)
11. Hsiung, C.C.: *A First Course in Differential Geometry*. John Wiley (1981)
12. Isihara, A.: Determination of molecular shape by osmotic measurement. *J. Chem. Phys.* **18**(11), 1446–1449 (1950)
13. Kaouche, A., Leroux, P.: Mayer and Ree-Hoover weights of infinite families of 2-connected graphs. *Seminaire Lotharingien de Combinatoire* **61 A**, B61Af (2009)
14. Kihara, T.: The second virial coefficient of non-spherical molecules. *J. Phys. Soc. Japan* **6**(5), 289–296 (1951)
15. Kihara, T.: Virial coefficients and models of molecules in gases. *Rev. Mod. Phys.* **25**, 831–843 (1953)
16. Korden, S.: Beyond the Rosenfeld functional: Loop contributions in fundamental measure theory (2012)
17. Korden, S.: Deriving the Rosenfeld functional from the virial expansion. *Phys. Rev. E* **85**(4), 041,150 (2012)
18. Marechal, M., Goetze, H.H., Härtel, A., Löwen, H.: Inhomogeneous fluids of colloidal hard dumbbells: Fundamental measure theory and monte carlo. *J. Chem. Phys* **135**, 234,510 (2011)
19. Marechal, M., Korden, S., Mecke, K.: Deriving fundamental measure theory: Reconciling the zero-dimensional limit with the virial approach, in preparation
20. Marechal, M., Löwen, H.: Density functional theory for hard polyhedra. *Phys. Rev. Lett.* **110**, 137,801 (2013)
21. Marechal, M., Zimmermann, U., Löwen, H.: Freezing of parallel hard cubes with rounded edges. *J. Chem. Phys.* **136**(14), 144,506 (2012)
22. McDonald, I.R., Hansen, J.P.: *Theory of Simple Liquids*. University of Cambridge (2008)
23. Minkowski, H.: Volumen und oberfläche. *Math. Ann.* **57**, 447–495 (1903)
24. Ree, F.H., Hoover, W.G.: Fifth and sixth virial coefficients for hard spheres and hard disks. *J. Chem. Phys.* **40**, 939 (1964)
25. Ree, F.H., Hoover, W.G.: Reformulation of the virial series of classical fluids. *J. Chem. Phys* **41**, 1635 (1964)
26. Ree, F.H., Hoover, W.G.: Seventh virial coefficients for hard spheres and hard disks. *J. Chem. Phys* **46**, 4181 (1967)
27. Ree, F.H., Keeler, R.N., McCarthy, S.L.: Radial distribution function of hard spheres. *J. Chem. Phys* **44**, 3407 (1966)
28. Reiss, H., Frisch, H.K., Lebowitz, J.L.: Statistical mechanics of rigid spheres. *J. Chem. Phys.* **31**(2), 369–380 (1959)
29. Riddell, R.J., Uhlenbeck, G.E.: On the theory of the virial development of the equation of the state of monoatomic gases. *J. Chem. Phys.* **21**, 2056 (1953)
30. Rosenfeld, Y.: Scaled field particle theory of the structure and the thermodynamics of isotropic hard particle fluids. *J. Chem. Phys.* **89**(7), 4272–4287 (1988)
31. Rosenfeld, Y.: Free-energy model for the inhomogeneous hard-sphere fluid mixture and density-functional theory of freezing. *Phys. Rev. Lett.* **63**(9), 980–983 (1989)
32. Rosenfeld, Y.: Density functional theory of molecular fluids: Free-energy model for the inhomogeneous hard-body fluid. *Phys. Rev. E* **50**(5), R3318–R3321 (1994)
33. Rosenfeld, Y.: Free energy model for the inhomogeneous hard-body fluid: Application of the Gauss-Bonnet theorem. *Mol. Phys.* **86**, 637–647 (1995)
34. Rosenfeld, Y., Levesque, D., Weis, J.: Free-energy model for the inhomogeneous hard-sphere fluid mixture - triplet and higher-order direct correlation-functions in dense fluids. *J. Chem. Phys.* **92**(11), 6818–6832 (1990)
35. Rosenfeld, Y., Schmidt, M., Löwen, H., Tarazona, P.: Dimensional crossover and the freezing transition in density functional theory. *J. Phys.: Condens. Matter* **8**, L577–L581 (1996)
36. Rosenfeld, Y., Schmidt, M., Löwen, H., Tarazona, P.: Fundamental-measure free-energy density functional for hard-spheres: Dimensional crossover and freezing. *Phys. Rev. E* **55**, 4245–4263 (1997)
37. Roth, R.: Fundamental measure theory for hard-sphere mixtures: A review. *J. Phys.: Condens. Matter* **22**, 063,102–063,120 (2010)
38. Roth, R., Evans, R., Lang, A., Kahl, G.: Fundamental measure theory for hard-sphere mixtures revisited: The white bear version. *J. Phys.: Condens. Matter* **14**, 12,063–12,078 (2002)
39. Santalo, L.A.: *Integral Geometry and Geometric Probability*. Addison-Wesley (1976)
40. Santos, A.: Class of consistent fundamental-measure free energies for hard-sphere mixtures. *Phys. Rev. E* **86**, 040,102 (2012)
41. Santos, A.: Note: An exact scaling relation for truncatable free energies of polydisperse hard-sphere mixtures. *J. Chem. Phys.* **136**, 136,102 (2012)

42. Schmidt, M.: Fluid structure from density-functional theory. *Phys. Rev. E* **62**(4), 4976–4981 (2000)
43. Schneider, R., Weil, W.: *Stochastic and Integral Geometry*. Springer (2008)
44. Tarazona, P.: Density functional for hard sphere crystals: A fundamental measure approach. *Phys. Rev. Lett.* **84**, 694–697 (2000)
45. Tarazona, P., Rosenfeld, Y.: From zero-dimensional cavities to free-energy functionals for hard disks and hard spheres. *Phys. Rev. E* **55**, R4873–R4876 (1997)
46. Uhlenbeck, G.E., Ford, G.W.: *The Theory of Linear Graphs with Applications to the Theory of the Virial Development of the Properties of Gases*, *Studies in Statistical Mechanics*, vol. 1. Interscience Publishers (1962)
47. Wertheim, M.S.: Fluids of hard convex molecules I. basic theory. *Mol. Phys.* **83**, 519–537 (1994)
48. Wertheim, M.S.: Fluids of hard convex molecules II. two-point measures. *Mol. Phys.* **89**, 989–1004 (1996)
49. Wertheim, M.S.: Fluids of hard convex molecules III. the third virial coefficient. *Mol. Phys.* **89**, 1005–1017 (1996)
50. Wertheim, M.S.: Third virial coefficient of hard spheroids. *Mol. Phys.* **99**, 187–196 (2001)